REPORT NO.
UCB/SEMM-89/19

STRUCTURAL ENGINEERING,
MECHANICS AND MATERIALS

A TRIANGULAR ELEMENT BASED ON REISSNER-MINDLIN PLATE THEORY

by

PANAYIOTIS PAPADOPOULOS

and

ROBERT L. TAYLOR

AUGUST 1989

DEPARTMENT OF CIVIL ENGINEERING
UNIVERSITY OF CALIFORNIA
BERKELEY, CALIFORNIA

A TRIANGULAR ELEMENT BASED ON REISSNER-MINDLIN PLATE THEORY

PANAYIOTIS PAPADOPOULOS[1] and *ROBERT L. TAYLOR*[2]

Department of Civil Engineering
University of California at Berkeley, Berkeley, CA, USA

ABSTRACT

A new triangular plate bending element based on the Reissner-Mindlin theory is developed through a mixed formulation emanating from the Hu-Washizu variational principle. A main feature of the formulation is the use of a linear transverse shear interpolation scheme with discrete constraint conditions on the edges. The element is shown to avoid shear locking, converge to the Kirchhoff plate theory as the plate thickness approaches zero, and generally exhibit excellent behavior on a series of standard problems and tests.

INTRODUCTION

Even though the problem of plate bending was originally tackled with the finite element method in the sixties, [1], it is widely accepted that the current state-of-the art allows for significant improvements to be made. During the present decade, many new finite element formulations have been introduced in a continuous attempt to attain satisfactory numerical treatment of the plate theories.

At the early stages of this process, interest was mainly oriented towards the classical plate theory that neglects shear deformation, usually referred to as Kirchhoff theory. However, the requirement of C^1 continuity of the shape functions, needed to guarantee the existence of the integral expression for the stiffness matrices, made researchers turn to theories of shear deformable plates, e.g. the theories of Reissner, [2], or Mindlin, [3]. Here, only C^0 continuity is required, consequently shape functions are considered easier to construct. This treatment, however, soon brought up the problem of shear locking, typical of formulations where overconstraining occurs.

Initially, locking was eliminated by using reduced integration schemes for the shear part of the stiffness, [4,5]. This obviously results in lower number of constraints and can be effective in many cases. It has to be pointed out though, that selective reduced integration may lead to singular behavior (rank deficiency), which is also undesirable (e.g., see [6]).

During the seventies and eighties, mixed variational formulations, [7], gave new insight to the treatment of many classes of problems with constraints, including plate bending and provided the basis for the development of new effective finite elements. Malkus and Hughes, [8], demonstrated the equivalence between some selective reduced integration

---

[1] *Graduate Research Assistant*

[2] *Professor*

and mixed formulations.

Two main directions emerged in the plate bending finite element literature within the context of mixed interpolations. The first, focused on overcoming the difficulty of C^1 continuity requirement of Kirchhoff's bending theory by imposing the zero-shear constraint in a discrete manner. The attempt was successful, [9], and a popular element, known as the DKT (Discrete Kirchhoff Triangle), appeared, [10]. The second approach developed thick plate elements using smooth shear strain fields together with appropriate discrete constraints, [11,12]. Finally, the incompatible element of Arnold and Falk, [13], is notable, since it has been shown to exhibit uniform convergence (for a restricted class of boundary conditions) in the context of Sobolev spaces.

In this paper, a "thick" plate approach is considered. This work is an extension to results presented in [15]. A key feature of the proposed element is the mixed interpolation of the transverse shear strain. A rotational degree of freedom is introduced for every edge to permit interpolation of rotations by (incomplete) quadratic functions, while the transverse displacement is interpolated cubically (also incompletely). Extensive tests demonstrate that the element:

(1) avoids shear locking and passes the patch test,

(2) is very accurate,

(3) is insensitive to geometric distorsions,

(4) provides stable solutions,

(5) converges to Kirchhoff solutions as the plate thickness goes to zero ("thin" plate limit),

(6) is applicable to a wide range of static and dynamic problems.

1. THE REISSNER-MINDLIN PLATE BENDING THEORY

In this work we use the simplest plate formulation which accounts for the effects of shear deformation. The assumptions of the theory are as follows:

(i) The domain Ω of the plate is of the form

$$\Omega = \left\{ (x,y,z) \in R^3 \;\middle|\; z \in [-\tfrac{1}{2}t, \tfrac{1}{2}t] \;,\; (x,y) \in A \subset R^2 \right\}$$

(ii) $$\sigma_{33} = 0$$

(iii) $$u = z\,\theta_y(x,y) \;,\; v = -z\,\theta_x(x,y) \;,\; w = w(x,y) \;,$$

where θ_x and θ_y are the rotations of transverse line elements about the x and y axes, respectively (e.g. see [14]). Assumption (iii) implies that straight normals to the reference surface, (z=0), remain straight, but do not necessarily remain normal to it after

deformation takes place. Also the transverse displacement w does not depend upon the thickness. Assumption (ii) is obviously inconsistent with three-dimensional elasticity. However, the transverse normal stress may be neglected for plates where the thickness is small compared with the other dimensions. The constitutive equations are required to satisfy the plane stress conditions.

A more refined theory (e.g. the Reissner theory, [2]) accounts for transverse warping and nonzero σ_{33} stress. However, these effects will not influence significantly the overall finite element analysis and thus are not included in this work.

The assumed displacement field (iii) yields in-plane strains of the form

$$\epsilon_x = z\,\theta_{y,x} \quad , \quad \epsilon_y = -z\,\theta_{x,y} \quad , \quad \gamma_{xy} = z\,(\theta_{y,y} - \theta_{x,x}) \tag{1.1}$$

and transverse shear strains

$$\gamma_{xz} = w_{,x} + \theta_y \quad , \quad \gamma_{yz} = w_{,y} - \theta_x \tag{1.2}$$

The above strain field for plane stress and isotropic linear elasticity gives in-plane stresses

$$\sigma_x = \frac{E}{1-\nu^2}[\epsilon_x + \nu\epsilon_y] \ ,$$

$$\sigma_y = \frac{E}{1-\nu^2}[\epsilon_y + \nu\epsilon_x] \ ,$$

$$\sigma_{xy} = \sigma_{yx} = G\gamma_{xy}$$

Similarly, the out-of-plane stresses are given by

$$\sigma_{xz} = \sigma_{zx} = G\gamma_{xz} \ ,$$

$$\sigma_{yz} = \sigma_{zy} = G\gamma_{yz} \ ,$$

where $G = \dfrac{E}{2(1+\nu)}$. Integrating the in-plane stresses, which vary linearly along the plate thickness, gives stress resultants (moments) of the following form :

$$M_x = \int_{-\frac{t}{2}}^{\frac{t}{2}} \sigma_x z dz \quad , \quad M_y = \int_{-\frac{t}{2}}^{\frac{t}{2}} \sigma_y z dz \quad , \quad M_{xy} = M_{yx} = \int_{-\frac{t}{2}}^{\frac{t}{2}} \sigma_{xy} z dz \tag{1.3}$$

At this point, we introduce the matrix notation

$$\mathbf{M} = \begin{bmatrix} M_x & M_y & M_{xy} \end{bmatrix}^T$$

and

$$\boldsymbol{\kappa} = \begin{bmatrix} \theta_{y,x} & -\theta_{x,y} & \theta_{y,y} - \theta_{x,x} \end{bmatrix}^T$$

It follows that the moment-curvature relation may be expressed as

$$\mathbf{M} = \mathbf{D}\boldsymbol{\kappa} \ , \tag{1.4}$$

where

$$\mathbf{D} = E\frac{t^3}{12(1-\nu^2)}\begin{bmatrix}1 & \nu & 0\\ \nu & 1 & 0\\ 0 & 0 & (1-\nu)/2\end{bmatrix}$$

Similarly, the out-of-plane stresses, when integrated along the thickness, give transverse shear forces

$$S_x = \int_{-\frac{t}{2}}^{\frac{t}{2}} \sigma_{xz}\,dz \quad , \quad S_y = \int_{-\frac{t}{2}}^{\frac{t}{2}} \sigma_{yz}\,dz \tag{1.5}$$

In short-hand notation we may again write

$$\mathbf{S} = Gt\boldsymbol{\gamma} = \alpha\boldsymbol{\gamma} \quad , \tag{1.6}$$

where

$$\mathbf{S} = \begin{bmatrix}S_x & S_y\end{bmatrix}^T \quad , \quad \boldsymbol{\gamma} = \begin{bmatrix}w_{,x} + \theta_y & w_{,y} - \theta_x\end{bmatrix}^T$$

Summation convention is implied over x,y,z for Latin indices and over x,y for Greek indices, so that the local equilibrium equations may be appropriately integrated through the thickness to deduce the plate equilibrium equations

$$M_{\alpha\beta,\beta} - S_\alpha = 0 \quad , \quad S_{\alpha,\alpha} + q = 0 \quad , \tag{1.7}$$

where q denotes the transverse surface loading. The first equation of equilibrium relates the bending moments to the shear forces, whereas the second one is a statement of transverse force equilibrium.

In the limiting case where $t \to 0$ the Kirchhoff hypothesis of zero transverse shear strain must hold. Hence

$$w_{,x} + \theta_y = 0 \quad , \quad w_{,y} - \theta_x = 0$$

Equations (1.2) imply that the transverse shear strain remains constant throughout the thickness. This is inconsistent with classical theory, where the corresponding transverse shear stress varies quadratically. Consequently, we may make a temporary modification to the displacement field, namely

$$u = z\theta_y + (z^3 + \beta z)\phi\,(x,y) \tag{1.8}$$

We impose the constraint

$$\int_{-\frac{t}{2}}^{\frac{t}{2}} (z^3 + \beta z)z\,dz = 0$$

and $\gamma_{xz} = 0$ on the plate faces to obtain

$$\gamma_{xz} = [1 - \frac{5}{3t^2}(3z^2 - \frac{3t^2}{20})](\theta_y + w_{,x}) \tag{1.9}$$

Moreover, substituting (1.9) into (1.6) we get

$$S_x = \int_{-\frac{t}{2}}^{\frac{t}{2}} G\gamma_{xz}\,dz = G(\theta_y + w_{,x}) \int_{-\frac{t}{2}}^{\frac{t}{2}} [1 - \frac{5}{3t^2}(3z^2 - \frac{3t^2}{20})]dz = \frac{5}{6}G(\theta_y + w_{,x})$$

Hence, for consistency reasons, we incorporate a "shear correction" term

$$\kappa = \frac{5}{6}$$

into equation (1.6), which now becomes

$$\mathbf{S} = \frac{5}{6}\alpha\boldsymbol{\gamma} = \bar{\alpha}\boldsymbol{\gamma} \quad , \tag{1.10}$$

where $\bar{\alpha} = \frac{5}{6}Gt$ and is used in this form hereafter.

For the purpose of the finite element approximation in the next section, we introduce a mixed variational form of the problem, based on the total potential energy for bending and on the Hu-Washizu principle for the transverse shear energy. Accordingly,

$$\Pi_1(\boldsymbol{\theta}, w, \mathbf{S}, \boldsymbol{\gamma}) = \frac{1}{2}\int_A \boldsymbol{\kappa}^T(\boldsymbol{\theta})\mathbf{D}\boldsymbol{\kappa}(\boldsymbol{\theta})dA + \frac{1}{2}\int_A \boldsymbol{\gamma}^T\bar{\alpha}\boldsymbol{\gamma}dA - \tag{1.11}$$

$$-\int_A \mathbf{S}^T(\boldsymbol{\gamma} - \nabla w - \mathbf{e}\boldsymbol{\theta})dA - \int_A wqdA + \Pi_{ext} \quad ,$$

where $\mathbf{e}$ is the alternating tensor

$$\mathbf{e} = \begin{bmatrix} 0 & 1 \\ -1 & 0 \end{bmatrix}$$

and Π_{ext} decribes the effect of boundary and other loads.

Taking the variation of Π_1 with respect to $\mathbf{S}$ and setting it equal to zero, we get

$$\int_A \delta\mathbf{S}^T(\boldsymbol{\gamma} - \nabla w - \mathbf{e}\boldsymbol{\theta})dA = 0 \quad , \tag{1.12}$$

which must be viewed as a constraint equation.

In the limiting case of $\boldsymbol{\gamma} \to 0$, the functional in (1.11) becomes

$$\Pi_1(\boldsymbol{\theta}, w, \mathbf{S}) = \frac{1}{2}\int_A \boldsymbol{\kappa}^T(\boldsymbol{\theta})\mathbf{D}\boldsymbol{\kappa}(\boldsymbol{\theta})dA + \tag{1.13}$$

$$+ \int_A \mathbf{S}^T(\nabla w + \mathbf{e}\boldsymbol{\theta})dA - \int_A wqdA + \Pi_{ext}$$

Pointwise satisfaction of (1.12) leads to a displacement formulation with the total potential energy functional given by

$$\Pi(\boldsymbol{\theta}, w) = \frac{1}{2}\int_A \boldsymbol{\kappa}^T\mathbf{D}\boldsymbol{\kappa}dA + \frac{1}{2}\int_A \boldsymbol{\gamma}^T\bar{\alpha}\boldsymbol{\gamma}dA - \int_A wqdA + \Pi_{ext} \quad , \tag{1.14}$$

whereas the weak form (1.11) is exploited in performing mixed finite element approximations described below.

2. FINITE ELEMENT APPROXIMATION

The fields $\boldsymbol{\theta} = [\theta_x, \theta_y]^T$, w, S and $\boldsymbol{\gamma}$ are considered as independent variables, in (1.11). Therefore, independent approximation schemes may be used for each field. In the general case we will assume an approximation

$$\boldsymbol{\theta} = \mathbf{N}_\theta \hat{\boldsymbol{\theta}} \ , \tag{2.1}$$

$$w = \mathbf{N}_w \hat{\mathbf{w}} + \mathbf{N}_{w\theta} \hat{\boldsymbol{\theta}} \tag{2.2}$$

and

$$\boldsymbol{\gamma} = \mathbf{N}_\gamma \hat{\boldsymbol{\gamma}} \ , \tag{2.3}$$

where $\hat{\boldsymbol{\theta}}$, $\hat{\mathbf{w}}$ and $\hat{\boldsymbol{\gamma}}$ are the nodal values of each variable, respectively. In addition, S will be approximated by

$$\mathbf{S} = \mathbf{S}(\boldsymbol{\theta}, w) = \sum_{k=1}^{3} \delta(\mathbf{x} - \mathbf{x}_k) \mathbf{t}_k \bar{S}_t^k \ ,$$

where δ is the Dirac function, $\mathbf{t}_k$ is the tangent to the element side and $\bar{S}_t^k$ is the tangential shear stress at the midpoint k of the element side.

Taking into account the constraint equation (1.14) along with the above interpolation for S, equation (2.3) becomes (e.g., see [15])

$$\hat{\boldsymbol{\gamma}} = \mathbf{Q}_\theta \hat{\boldsymbol{\theta}} + \mathbf{Q}_w \hat{\mathbf{w}} \tag{2.4}$$

Note that, due to this constraint equation, $\hat{\boldsymbol{\gamma}}$ is no longer an independent variable.

It is important to point out that the constraint equation will be satisfied only in a discrete sense, i.e. only at appropriately chosen parts of the boundary. Accordingly, this is essentially a Discrete Reissner-Mindlin plate formulation (DRM).

Upon substitution of (2.1) (2.2) and (2.4) into (1.11), we get

$$\Pi_1 = \frac{1}{2}\int_A (\mathbf{L}\mathbf{N}_\theta \hat{\boldsymbol{\theta}})^T \mathbf{D} (\mathbf{L}\mathbf{N}_\theta \hat{\boldsymbol{\theta}}) dA \ + \tag{2.5}$$

$$+ \ \frac{1}{2}\int_A (\mathbf{N}_\gamma \mathbf{Q}_\theta \hat{\boldsymbol{\theta}} + \mathbf{N}_\gamma \mathbf{Q}_w \hat{\mathbf{w}})^T \bar{\alpha} [\mathbf{N}_\gamma \mathbf{Q}_\theta \hat{\boldsymbol{\theta}} + \mathbf{N}_\gamma \mathbf{Q}_w \hat{\mathbf{w}}] dA \ - \int_A (\mathbf{N}_w \hat{\mathbf{w}} + \mathbf{N}_{w\theta} \hat{\boldsymbol{\theta}})^T q dA \ + \Pi_{ext} \ ,$$

where L is a differential operator defined by

$$\mathbf{L} = \begin{bmatrix} 0 & -\frac{\partial}{\partial y} & -\frac{\partial}{\partial x} \\ \frac{\partial}{\partial x} & 0 & \frac{\partial}{\partial y} \end{bmatrix}^T$$

Minimization of (2.5) with respect to $\hat{\theta}$ and $\hat{w}$ leads to a matrix equation of the form

$$\begin{bmatrix} \mathbf{K}_{\theta\theta} & \mathbf{K}_{\theta w} \\ \mathbf{K}_{w\theta} & \mathbf{K}_{ww} \end{bmatrix} \begin{Bmatrix} \boldsymbol{\theta} \\ \mathbf{w} \end{Bmatrix} = \begin{bmatrix} \mathbf{f}_\theta \\ \mathbf{f}_w \end{bmatrix} \quad ,$$

where

$$\mathbf{K}_{\theta\theta} = \int_A \{[\mathbf{L}\mathbf{N}_\theta]^T \mathbf{D}[\mathbf{L}\mathbf{N}_\theta] + [\mathbf{N}_\gamma \mathbf{Q}_\theta]^T \bar{\alpha}[\mathbf{N}_\gamma \mathbf{Q}_\theta]\} dA \quad , \tag{2.6}$$

$$\mathbf{K}_{\theta w} = \mathbf{K}_{w\theta}^T = \int_A [\mathbf{N}_\gamma \mathbf{Q}_w]^T \bar{\alpha}[\mathbf{N}_\gamma \mathbf{Q}_\theta] dA \quad , \tag{2.7}$$

$$\mathbf{K}_{ww} = \int_A [\mathbf{N}_\gamma \mathbf{Q}_w]^T \bar{\alpha}[\mathbf{N}_\gamma \mathbf{Q}_w] dA \tag{2.8}$$

and

$$\mathbf{f}_\theta = \int_A \mathbf{N}_{w\theta}^T q dA \quad , \quad \mathbf{f}_w = \int_A \mathbf{N}_w^T q dA \tag{2.9}$$

External forces are also affected by Π_{ext}.

3. FINITE ELEMENT FORMULATION - A NEW TRIANGULAR ELEMENT

A new triangular plate bending finite element is developed based upon the approximation described in the previous section. Following the approach used in [15] and [16], θ is assumed to vary quadratically (although not all quadratic terms are present) in each element, according to the following interpolation, Fig. (3.1),

$$\theta = \sum_{i=1}^{3} L_i \hat{\theta}_i + \sum_{i=1}^{3} 4 L_i L_j \mathbf{n}_k \Delta\hat{\theta}_k \quad , \tag{3.1}$$

where j = mod(i,3) + 1 , k = mod(j,3) + 1 , L_i are the standard area coordinates, [17], and $\mathbf{n}_k$ is the normal to the edge k. It should be noted that the interpolation for each edge degree of freedom is hierarchical.

In addition, w is assumed to vary cubically (also incompletely), according to

$$w = \sum_{i=1}^{3} L_i \hat{w}_i + \sum_{i=1}^{3} 4 L_i L_j (\alpha_k L_i + \beta_k L_j) \quad , \tag{3.2}$$

where the parameters α_l, β_l, l=1,2,3 are to be determined by requiring the tangential shear strain to be *constant along each edge of the triangle*. Imposing the above constraints yields

$$\alpha_i = \pm \left\{ \frac{l_i}{8}[(\theta_{y_j} - \theta_{y_i})\sin\omega_i + (\theta_{x_j} - \theta_{x_i})\cos\omega_i] + \frac{-l_i}{6}\Delta\theta_i \right\} \tag{3.3}$$

$$\beta_i = \pm \left\{ \frac{l_i}{8}[(\theta_{y_j} - \theta_{y_i})\sin\omega_i + (\theta_{x_j} - \theta_{x_i})\cos\omega_i] + \frac{l_i}{6}\Delta\theta_i \right\} \tag{3.4}$$

where ω_i is shown in Fig. (3.2).

In the above equations, the sign attached to α_i , β_i is determined once a unique boundary direction is selected. Detailed derivation of the above result may be found in Appendix A. Special care must be taken in order to guarantee a unique definition of the positive direction along every edge. Failure to achieve this, results in inconsistent definition of the edge rotational degrees of freedom.

Substitution of (3.1) to (3.4) in (A.5) gives the constant tangential shear along the edge i-j

$$\gamma_{tz} = \pm \frac{1}{l_{ij}}(w_j - w_i) - \frac{1}{2}[(\theta_{y_i} + \theta_{y_j})\sin\omega_k + (\theta_{x_i} + \theta_{x_j})\cos\omega_k] - \frac{2}{3}\Delta\theta_k$$

Finally, the out-of-plane shear strain field is assumed to be linear

$$\gamma = \sum_{i=1}^{3} L_i \hat{\gamma}_i \quad ,$$

where $\hat{\gamma}_i$ are to be determined by satisfying the discrete edge constraints of constant tangent shear strain. Along the generic edge i-j, Fig. (3.2), the constraint conditions are

$$\frac{1}{2}(\hat{\gamma}_i + \hat{\gamma}_j).\mathbf{t}_k = \gamma_{tz} = C_i$$

and

$$\frac{1}{2}(\hat{\gamma}_i - \hat{\gamma}_j).\mathbf{t}_k = 0 \quad ,$$

where $\mathbf{t}_i$ is the tangent vector to the j-k edge The above equations may be rewritten as

$$C_i = \hat{\gamma}_i.\mathbf{t}_k = \hat{\gamma}_j.\mathbf{t}_k \quad ,$$

where i,j,k satisfy the modulo expressions defined above. Note that with the above convention

$$\mathbf{t}_i = [-\sin\omega_i \quad \cos\omega_i]^T = [t_{ix} \quad t_{iy}]^T$$

The above six equations we obtain (2 per edge) may be solved for the values of $\hat{\gamma}_i$, i = 1,2,3 (e.g., see [13]).

Hence,

$$\hat{\gamma}_i = \begin{Bmatrix} \hat{\gamma}_{ix} \\ \hat{\gamma}_{iy} \end{Bmatrix} = \frac{1}{\delta_i} \begin{Bmatrix} t_{jy}C_k - t_{ky}C_j \\ t_{kx}C_j - t_{jx}C_k \end{Bmatrix} \quad , \tag{3.5}$$

where

$$\delta_i = t_{kx}t_{jy} - t_{ky}t_{jx} \tag{3.6}$$

The strain-displacement matrices due to bending, B_b, and shear, B_s, are easily obtained

using the above results. The element stiffness matrix then may be computed as

$$\mathbf{K} = \int_A \mathbf{B}_b{}^T \mathbf{D} \mathbf{B}_b \, dA \;+\; \int_A \mathbf{B}_s{}^T \bar{\alpha} \mathbf{B}_s \, dA \tag{3.7}$$

The load vector also may be computed consistently using (2.9). As an alternative option, a "lumped" load vector is also computed by ignoring the dependence of the transverse displacement on the rotational degrees of freedom. In the numerical applications, the consistent loading will be shown to behave better than the "lumped". Since both the in-plane and the out-of-plane strains vary linearly along the element, a three point Gauss quadrature, [18], is sufficient for exact integration.

4. FINITE ELEMENT PROPERTIES

4.1 Locking

In recent finite element literature, conditions have been determined, under which an element displays the locking phenomenon.

A quick and generally reliable method of assessing element performance with regard to locking calls for a simple constraint count, [15,19,20], as below; we define n_θ,n_w and n_γ as the number of variables involved in the interpolation of each one of θ, w and γ, respectively. In addition, interpolations for S with n_s independent parameters always satisfy

$$n_s = n_\gamma$$

Minimization of the functional in (1.13) gives rise to the following matrix system of equations to be satisfied in the thin plate limit :

$$\begin{bmatrix} \mathbf{A} & \mathbf{B} & \mathbf{0} \\ \mathbf{B}^T & \mathbf{0} & \mathbf{C} \\ \mathbf{0} & \mathbf{C}^T & \mathbf{0} \end{bmatrix} \begin{bmatrix} \hat{\theta} \\ \bar{\mathbf{S}} \\ \hat{\mathbf{w}} \end{bmatrix} = \begin{bmatrix} \mathbf{f}_\theta \\ \mathbf{0} \\ \mathbf{f}_w \end{bmatrix} , \tag{4.1}$$

where

$$\mathbf{A} = \int_A [\mathbf{L}\mathbf{N}_\theta]^T \mathbf{D} [\mathbf{L}\mathbf{N}_\theta] dA \quad ,$$

$$\mathbf{B} = \int_A [\nabla \mathbf{N}_{w\theta}^T \mathbf{N}_s + (\mathbf{e}\mathbf{N}_\theta)^T \mathbf{N}_s] dA \quad ,$$

$$\mathbf{C} = \int_A \mathbf{N}_s^T \nabla \mathbf{N}_w \, dA$$

and $\mathbf{f}_\theta$, $\mathbf{f}_w$ as in (2.9).

Non-singularity of the system in (4.1) implies that

$$n_\theta + n_w \geq n_{\mathfrak{S}} \tag{4.2}$$

and

$$n_\gamma \geq n_w \tag{4.3}$$

are necessary conditions for solution of the limit problem on any element patch. These, however, are not sufficient conditions for convergence and here numerical testing is used to assess overall performance.

In the case of our element, the test is passed for a single element with all boundaries fixed, as well as with only the rigid body motion constrained, Fig. (4.1.1). The same count may be repeated successfully for patches consisting of more than one element.

4.2 Relation to the DKT family of elements

Recall that DKT elements, [10], are based on the minimization of the total potential energy, neglecting the shear part, namely

$$\Pi = \frac{1}{2}\int_A \kappa^T D\,\kappa dA \; - \int_A wqdA \; + \Pi_{ext} \;,$$

subject to the constraint

$$\gamma = \frac{S}{\bar{\alpha}} = 0$$

along the edges.

The fact that in the present formulation, the same type of constraint is applied (here γ = constant along the edges), together with the inclusion of the shear energy, which approaches zero as t→0 can explain why the element converges to the DKT in the limit of the thin plate. The numerical results will verify this claim, as will be evident in the next chapter. Of course, to obtain a complete agreement in the thin limit, the nodal forces applied from uniform loads, q, must be the same for the two formulations.

4.3 A brief discussion of the boundary conditions

The boundary conditions of a clamped edge are universally accepted to be

$$w = \theta_n = \theta_s = 0 \;,$$

as illustrated in Fig. (4.3.1). A simply supported edge, on the other hand, may be approximated in more than one way. Thus we have

(1) "soft" simply supported edge (SS1)

$$w = 0 \;,\; M_n = 0 \;\text{ and }\; M_s = 0$$

and

(2) "hard" simply supported edge (SS2)

$$w = 0 \;,\; \theta_n = 0 \;\text{ and }\; M_s = 0$$

It can be easily deduced that the "hard" simply supported conditions are suitable for the thin plate limit. In most of the literature, the "soft" conditions are being used, because they are free of deficiencies concerning well-possedness of the problem for curved boundaries. A detailed discussion is given in [14]. In the present formulation an additional difficulty occurs. Specifically, the soft boundary conditions lead to a situation, where the transverse displacement is not equal to zero pointwise. This can be easily deduced from eq.(3.2). However, it is evident that w converges to zero in a weak sense, when the mesh is refined.

5. NUMERICAL PERFORMANCE

A series of numerical tests have been conducted in order to assess the performance of the new triangle. The new element with cubic transverse displacement (which in the sequel will be referred to as DRM3) has been incorporated into the Finite Element Analysis Program (FEAP), (e.g., see Chapter 15 of [17]) and all computations have been conducted within the FEAP environment. All results are compared to exact or approximate solutions as well as to results obtained with other elements. In addition, patch tests were conducted on the square plate of arbitrary triangles shown in Fig. (5.1). The tests include:

(i) pure bending (distributed constant edge moments along one edge, the opposite clamped and all lateral boundary tangential ratations fixed),

(ii) pure shear (distributed constant edge forces on one edge, the opposite clamped, and all rotations fixed in order to prevent bending),

(iii) pure twist (distributed constant edge twisting moments along two adjacent sides the other two sides restrained with SS2 simply supported conditions).

All the above tests are passed.

5.1 Uniform loading on square plate

A quadrant of a square plate is modeled with different meshes, Fig. (5.1.1), and for simply supported and clamped boundary conditions. Both soft and hard boundary conditions are considered for the simply supported case. Loading is consistent with the w-interpolation used and two mesh orientations (labeled A and B) are examined. The results are reported in Table 5.1 below. The analytical solution (in a series form) for the thin plate limit may be found in [21]. For the hard (SS2) simply supported conditions a correction (also in series form) may be added.

Table 5.1 : Uniform Loading on Square Plate

Uniform Loading (x 10^{-4})						
	Simply Supported				Clamped	
	Soft		Hard			
Mesh	A	B	A	B	A	B
1×1	4.7896	3.9028	4.7881	3.9023	1.8921	1.0377
2×2	4.1876	4.1627	4.1860	4.1619	1.4834	1.2884
4×4	4.0998	4.1010	4.0968	4.0988	1.3285	1.2822
8×8	4.0788	4.0791	4.0731	4.0739	1.2834	1.2719
16×16	4.0773	4.0771	4.0667	4.0669	1.2718	1.2689
Series (thin)	4.0623	4.0623	4.0623	4.0623	1.260	1.260
Series (thick)			4.0644	4.0644		

The material properties of the plate are

$$E = 10.92 \quad , \quad \nu = 0.3 \, ,$$

the side length is a = 10, the uniform loading q = 1.0 and the thickness t = 0.1. Thus, a condition approaching the thin plate limit is expected and, indeed, achieved, as seen from Table 5.1 .

5.2 Circular plate under uniform loading

Due to symmetry, one quadrant of a circular plate has been discretized with different meshes, Fig. (5.2.1), and the results for both the clamped and the simply supported case are obtained for a thick (R/t = 5/1) and a relatively thin (R/t = 5/0.1) plate. The results are compared to the exact thick plate solution.

Table 5.2 : Circular Plate under Uniform Loading

Displacement w at the center				
Thickness	t = 0.1		t = 1.0	
boun. cond.	SS1	clamped	SS1	clamped
No. of elements				
6	41990.8	10104.5	43.75	11.79
24	40469.6	9914.03	42.27	11.69
96	39999.3	9826.49	41.78	11.61
384	39874.9	9796.08	41.65	11.57
1536	39842.9	9787.15	41.61	11.56
Exact solution	39831.5	9783.48	41.60	11.55

The properties of the plate are

$$E = 10.92 \quad , \quad \nu = 0.3 \, ,$$

and the uniform loading q = 1.0 .

5.3 Skew cantilever plates

Here three skew cantilever plates are analyzed using different meshes and orientations of the triangles, Fig. (5.3.1). The results are compared with those obtained in [22].

Table 5.3 : Skew cantilever plates

		w at 1 (x Et^3/qa^4)			w at 2 (x Et^3/qa^4)		
Mesh	β (o)	DRM3 A	DRM3 B	[22] B	DRM3 A	DRM3 B	[22] B
2×2	20	1.3557	1.5438	1.3808	1.0704	1.0782	1.0297
	40	1.0637	1.2955	1.0867	0.5329	0.6182	0.5255
	60	0.7416	0.8523	0.7370	0.1259	0.2133	0.1373
4×4	20	1.4024	1.4446	1.4233	1.0489	1.0388	1.0419
	40	1.1266	1.1777	1.1613	0.5381	0.5435	0.5429
	60	0.7814	0.7956	0.8186	0.1411	0.1551	0.1510
8×8	20	1.4204	1.4285	1.4297	1.0440	1.0386	1.0442
	40	1.1619	1.1646	1.1613	0.5426	0.5375	0.5468
	60	0.8192	0.7935	0.8502	0.1501	0.1437	0.1562
16×16	20	1.4269	1.4275	-	1.0436	1.0413	-
	40	1.1789	1.1720	-	0.5456	0.5411	-
	60	0.8435	0.8128	-	0.1553	0.1471	-

The plate properties are

$$E = 100 \quad , \quad \nu = 0.3 \, ,$$

the thickness is t = 4.0, the side length L = 100 and the load q = 1.0 .

It should be noted that the element in [22] is of higher order than the DRM3 (it has 22 dof's, while DRM3 has only 12). The table indicates that the DRM3 results are only slightly sensitive to the triangle orientation, especially in coarse meshes. Generally, convergence is attained more easily for the 20^o plate rather than the other two. This is expected, since for highly skewed plates the effect of the obtuse angle singularity becomes stronger.

5.4 Simply supported skew plate (30^o)

For a highly skewed simply supported, uniformly loaded plate ($\beta = 60^o$, $\theta = 30^o = 90^o - \beta$) the results obtained for a set of meshes are compared to those of other elements and to the solution given in [23] for the "thin" plate. Results for the DRM3 subjected to lumped and consistent loading are given. Two different thicknesses are considered and the boundary conditions are taken to be soft throughout the analysis. A typical mesh is shown in Fig. (5.4.1).

Table 5.4a : Simply supported skew plate (t=1.0)

Center Displacement					
Side Nodes	Tri-6R [15]	DRM3 (cons.)	DRM3 (lumped)	T1 [24]	QUAD9* [12]
3	0.04859	0.08203	0.06798	0.00279	-
5	0.05739	0.04861	0.04599	0.04282	-
9	0.04161	0.04385	0.04384	0.03899	0.04237
17	0.04299	0.04510	0.04494	0.04187	0.04302
33	0.04491	0.04572	0.04568	0.04410	-
Ref. [23]	0.04455	0.04455	0.04455	0.04455	0.04455

Table 5.4b : Simply supported skew plate (t=0.1)

Center Displacement			
Side Nodes	Tri-6R [15]	DRM3 (cons.)	QUAD9* [12]
3	48.47	81.53	-
5	57.19	52.30	-
9	39.78	47.00	41.61
17	37.83	45.96	39.42
33	39.28	45.53	-
Ref. [23]	44.55	44.55	44.55

Plate properties:

$$E = 10. \times 10^6 \ ; \ \nu = 0.3 \ ;$$

Side length a = 100 and uniform loading q = 1.0

5.5 Free vibration analysis

For dynamic applications the inertia effects may be included by replacing q in (2.9) by $q - \rho h \ddot{w}$. The second term then leads to the definition of the mass matrix (M3)

$$\mathbf{M} = \int_A \rho h \begin{bmatrix} \mathbf{N}_w^T \mathbf{N}_w & \mathbf{N}_w^T \mathbf{N}_{w\theta} \\ \mathbf{N}_{w\theta}^T \mathbf{N}_w & \mathbf{N}_{w\theta}^T \mathbf{N}_{w\theta} \end{bmatrix} dA$$

A "lumped" mass, (ML), may be computed using nodal quadrature (e.g., see [17], app. 8)

and yields the result

$$M = \frac{\rho hA}{3}\begin{bmatrix} I & 0 \\ 0 & 0 \end{bmatrix}$$

For the element using linear interpolation for w, which has been reported in [15], $N_{w\theta} = 0$. The consistent mass for this interpolation (M1) is a special case of the cubic integral result.

Table 5.5 shows results computed for a simply supported (hard) square plate mesh type B as in Fig. (5.1.1).

Table 5.5 : Frequencies of a simply supported plate

		frequencies ω^2 ($\times 10^{-2}$)					
		Modes of vibration					
Mesh	Mass	(1,1)	(1,3) + (3,1)	(1,3) - (3,1)	(3,3)	(1,5) + (5,1)	(1,5) - (5,1)
1×1	M3	0.03468					
	M1	0.04803					
	ML	0.02402					
2×2	M3	0.03840	1.0753	1.0047	2.5472		
	M1	0.04330	1.9112	1.4438	4.2305		
	ML	0.03444	0.6841	0.7219	1.4448		
4×4	M3	0.03879	1.0032	0.9825	3.0582	7.0703	7.0482
	M1	0.04006	1.2384	1.1503	4.0977	10.989	10.621
	ML	0.03770	0.9090	0.9362	2.7134	5.6589	5.8238
8×8	M3	0.03890	0.9795	0.9739	3.1153	6.6758	6.6721
	M1	0.03922	1.0346	1.0158	3.3942	7.5804	7.5737
	ML	0.03862	0.9557	0.9632	3.0281	6.3762	6.4355
16×16	M3	0.03893	0.9733	0.9719	3.1331	6.5704	6.5701
	M1	0.03901	0.9868	0.9824	3.2035	6.7881	6.7857
	ML	0.03886	0.9673	0.9693	3.1110	6.4978	6.5136
Exact		0.03896	0.9732	0.9732	3.1511	6.5700	6.5700

The material and geometric properties are as in section 5.1 . A 7-point quadrature is used for the integration of the mass matrix, [18].

Only the eigenvalues associated with doubly symmetric modes are computed. It is noted that the consistent mass matrix based on the cubic interpolation of w gives more

accurate results than the lumped matrix. Moreover, the results based on the linearly interpolated w are less accurate than the lumped approximation. Thus, it is evident that the cubic interpolation is especially beneficial for dynamic applications.

The eigenvalues associated with the (1,3) and (3,1) eigenmodes (similarly (1,5) and (5,1)) are theoretically equal. The finite element analysis exhibits a slight difference in these values, due to the fact that the computed eigenvalues correspond to linear combinations of the theoretical modes. In fact, both values converge to the exact solution.

CLOSURE

The trianglular conforming plate bending element presented here is representative of a broad class of elements that feature discrete transverse shear constraints on the boundaries within the context of the Hu-Washizu principle. The particular element overcomes shear-locking a-priori via the constraint count procedure and exhibits excellent numerical behavior in terms of accuracy and stability over a comprehensive set of static test problems and a single test for modes of free vibration. Finally it should be noted that the cubic interpolation for w may be effectively used to compute loads, mass and geometric stiffness for the DKT triangle.

REFERENCES

[1] R. W. Clough and J.L. Tocher, "Finite element stiffness matrices for analysis of plates in bending", Proc. Conf. on Matrix Methods in Structural Mechanics, AFFDL-TR-66-80, WPAFB, Ohio, 515-545, (1966).

[2] E. Reissner, "The effect of transverse shear deformation on the bending of elastic plates", J. Appl. Mech., 12, 69-76, (1945).

[3] R.D. Mindlin, "Influence of rotatory and shear on flexural motions of isotropic, elastic plates", J. Appl. Mech., 18, 31-38, (1951).

[4] O.C. Zienkiewicz, R.L. Taylor and J. Too, "Reduced integration technique in general analysis of plates and shells", Int. J. Num. Meth. Eng., 3, 275-290, (1971).

[5] S.F. Pawsey and R.W. Clough, "Improved numerical integrationof thick slab finite elements", Int. J. Num. Meth. Eng., 3, 575-586, (1971).

[6] T.J.R. Hughes, R.L. Taylor, and W. Kanoknukulchai, "A simple and efficient element for plate bending", Int. J. Num. Meth. Eng., 11, 1529-1543, (1977).

[7] K. Washizu, "Variational Methods in Elasticity and Plasticity", Oxford: Pergamon Press, (1982).

[8] D.S. Malkus and T.J.R. Hughes, "Mixed finite element methods-Reduced and selective integration techniques: A unification of concepts", Comp. Meth. Appl. mech.

Eng., 15, 63-81, (1978).

[9] G.A. Wempner, J.T. Oden and D.K. Dross, "Finite element analysis of thin shells", Proc. A.S.C.E., EM6, 1273-1294, (1968).

[10] J.-L. Batoz, K.-J. Bathe and L.-W. Ho, "A study of three-node triangular plate bending elements", Int. J. Num. Meth. Eng., 15, 1771-1812, (1980).

[11] K.-J. Bathe and E.N. Dvorkin, "A four-node plate bending element based on the Mindlin/Reissner plate theory and a mixed interpolation", Int. J. Num. Meth. Eng., 21,367-383, (1985).

[12] H.C. Huang and E. Hinton, "A nine-node Lagrangian Mindlin plate element with enhanced shear interpolation", Eng. Comp., 1, 369-379, (1984).

[13] D.N. Arnold and R.S Falk, " A uniformly accurate finite element method for the Mindlin-Reissner plate", IMA Preprint 307, (1987).

[14] T.J.R. Hughes, "The Finite Element Method", Englewood Cliffs, N.J.: Prentice-Hall, (1987).

[15] O.C. Zienkiewicz, R.L. Taylor, P. Papadopoulos and E. Onate, "Plate bending elements with discrete constraints: New triangular elements", UCB/SEMM Rep. 89/09, Dept. Civ. Engr., UCB, (1989).

[16] M.A. Chrisfield, "A four-noded thin-plate bending element using shear constraints - a modified version of Lyons' element", Comp. Meth. Appl. Mech. Eng., 38, 93-120, (1983).

[17] O.C. Zienkiewicz and R.L. Taylor, "The Finite Element Method", 4th ed., Vol. 1, McGraw-Hill, London, (1989).

[18] "Handbook of Mathematical Functions; with formulas, graphs, and mathematical tables", M. Abramowitz and I.A. Stegun editors, Dover, New York, (1970).

[19] O.C.Zienkiewicz and D. Lefebvre, "Three-node mixed approximation and the plate bending problem", Comm. Appl. Num. Meth., 3, 301-309, (1987).

[20] O.C. Zienkiewicz, S. Qu, R.L. Taylor, and S.Nakazawa, "The patch test for mixed formulations, Int. J. Num. Meth. Eng., 23, 1873-1883, (1986).

[21] S. Timoshenko and S. Woinowsky-Krieger, "Theory of Plates and Shells", McGraw-Hill, London, (1959).

[22] F.-G. Yuan and R.E. Miller, "A cubic triangular finite element for flat plates with shear", Int. J. Num. Meth. Eng., 28, 109-126, (1989).

[23] L.S.D. Morley, "Skew Plates and Structures", International Series of Monographs in Aeronautics and Astronautics, MacMillan, New York, (1963).

[24] T.J.R. Hughes and T.E. Tezduyar, "Finite elements based upon Mindlin plate theory with particular reference to the four node bilinear isoparametric element", J. Appl. Mech., 46, 587-596, (1981).

APPENDIX A : Derivation of the transverse displacement interpolation

The shear strain along the edges is calculated in a straightforward way as follows: Along the typical edge i-j, we have, Fig. (A.1),

$$\gamma_{tz} = \frac{\partial w}{\partial s} - (\theta_x \cos\omega_k + \theta_y \sin\omega_k) \quad , \tag{A.1}$$

where

$$\frac{\partial w}{\partial s} = \frac{\partial w}{\partial L_i}\frac{\partial L_i}{\partial s} \tag{A.2}$$

and

$$\frac{\partial w}{\partial L_i} = w_i + 4L_j(2\alpha_k L_i + \beta_k L_j) + 4L_k(\alpha_j L_k + 2\beta_j L_i) \tag{A.3}$$

For the choice of positive direction along the edge 1-2, as in the figure

$$\frac{\partial L_1}{\partial s} = -\frac{\partial L_2}{\partial s} = \frac{1}{l_{12}} \quad , \quad \frac{\partial L_3}{\partial s} = 0 \quad , \tag{A.4}$$

l_{12} being the length of the edge 1-2. Similar results may be obtained for the other edges.

After some algebraic manipulations, equation (A.1), with the use of (A.2), (A.3) and (A.4), becomes

$$\frac{\partial w}{\partial s} - \theta_n = \frac{1}{l_{12}}(w_2 - w_1) - \frac{1}{l_{12}}4\beta_3 - \theta_{x_2}\cos\omega_3 - \theta_{y_2}\sin\omega_3 + \tag{A.5}$$

$$+L_1[-\frac{8}{l_{12}}(\alpha_3 - \beta_3) + \frac{8}{l_{12}}\beta_3 - \theta_{x_1}\cos\omega_3 - \theta_{y_1}\sin\omega_3 + \theta_{x_2}\cos\omega_3 + \theta_{y_2}\sin\omega_3 - 4\Delta\theta_3] +$$

$$+4L_1^2[-\frac{1}{l_{12}}(2\alpha_3 + \beta_3) + \frac{1}{l_{12}}(\alpha_3 - 2\beta_3) + 4\Delta\theta_3]$$

Imposing the constant shear constraint along the edge, the coefficients of L_1 and L_1^2 must vanish, hence we obtain the following system of equations

$$\alpha_3 - \beta_3 = -\frac{l_{12}}{3}\Delta\theta_3 \quad ,$$

$$\alpha_3 - 2\beta_3 = -\frac{l_{12}}{8}[(\theta_{y_1} - \theta_{y_2})\sin\omega_3 + (\theta_{x_1} - \theta_{x_2})\cos\omega_3 + 4\Delta\theta_3] \quad ,$$

which, when solved, gives eq. (3.3) and (3.4). The same technique is employed for the other two edges edges of the triangular element, so that all six parameters α_k, β_k, k=1,2,3 are uniquely determined.

It is important to note that the values of the two parameters for every edge, depend only on the nodal values and the edge value along this edge, therefore continuity of tangential strains is satisfied along the interelement boundaries. Of course, this is not the case, in general, for the normal strains.

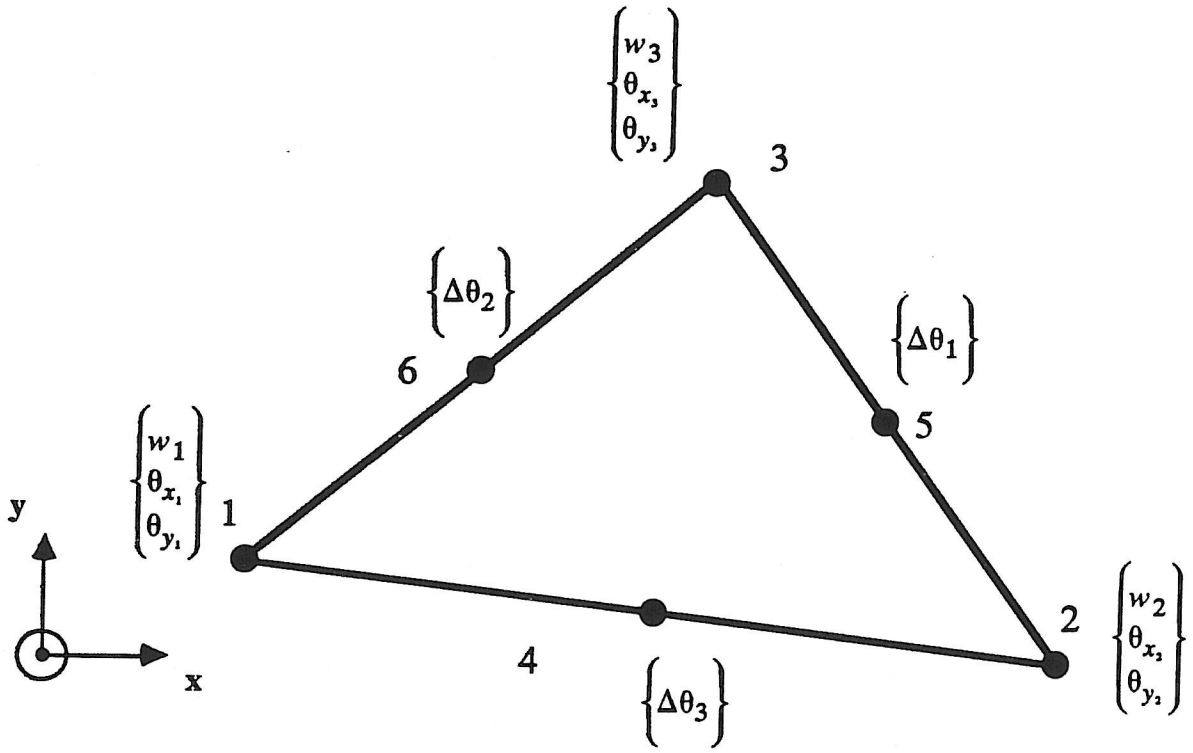

Fig. 3.1 Node and dof assignment for the triangular DRM3 element

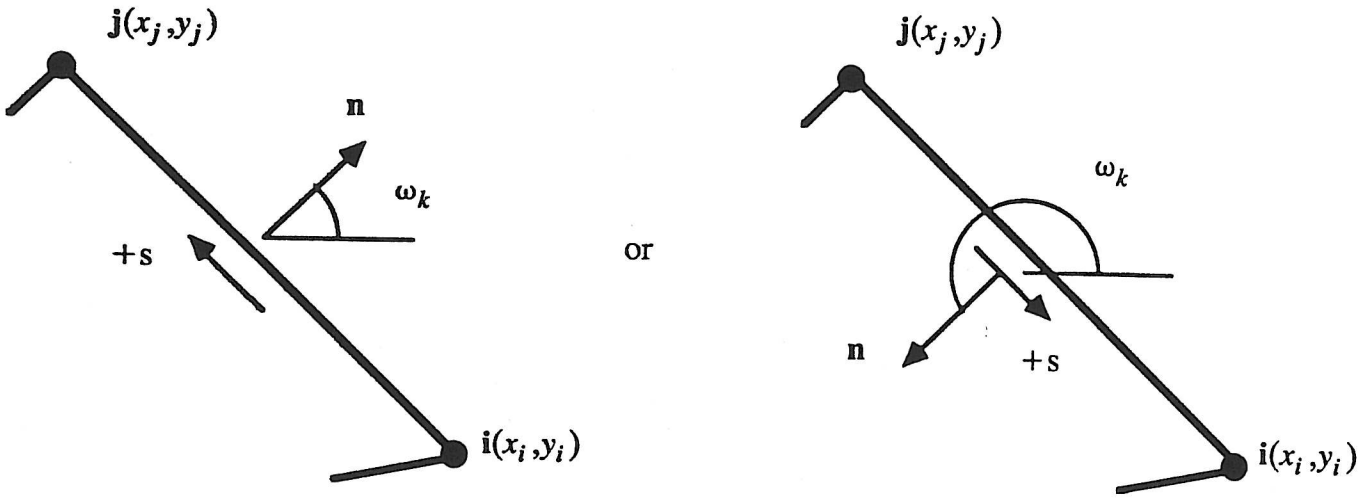

$$l_{ij} = [\ (x_i - x_j)^2 + (y_i - y_j)^2\ ]^{1/2}$$

$$\cos\omega_k = -(y_i - y_j)/l_{ij}$$
$$\sin\omega_k = (x_i - x_j)/l_{ij}$$

$$\cos\omega_k = -(y_j - y_i)/l_{ij}$$
$$\sin\omega_k = (x_j - x_i)/l_{ij}$$

Fig. 3.2 Geometric data and positive direction along an edge

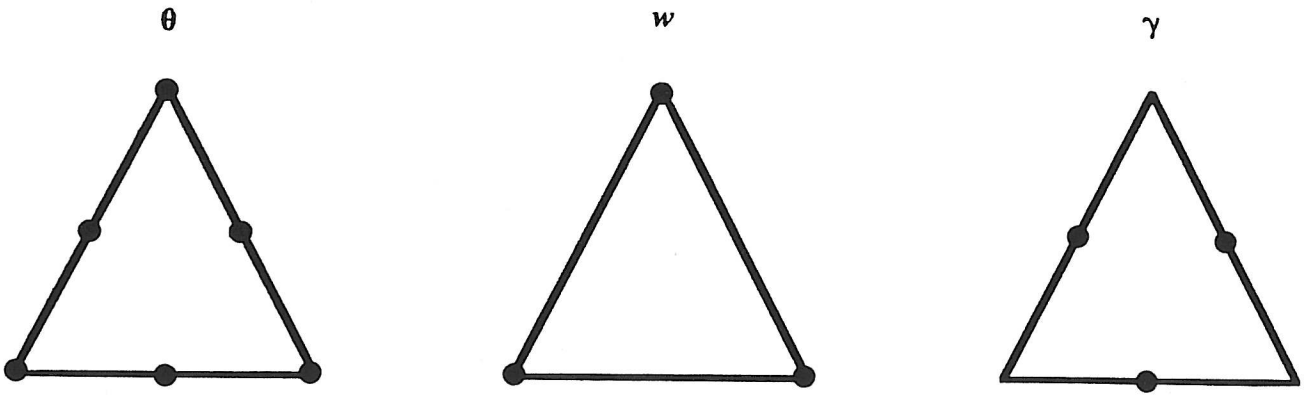

Test C:	$n_\theta = 0$	$n_w = 0$	$n_s = 0$
Test R:	$n_\theta = 9-2 = 7$	$n_w = 3-1 = 2$	$n_s = 3$

C: all boundary dofs constrained
R: rigid body motion constrained

Fig. 4.1.1 Constraint count for a single element

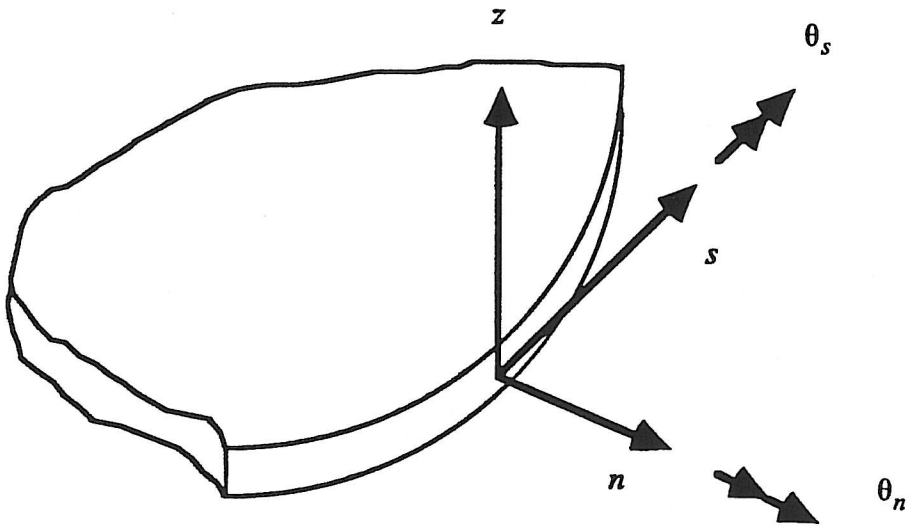

Fig. 4.3.1 Boundary conditions for a thick plate

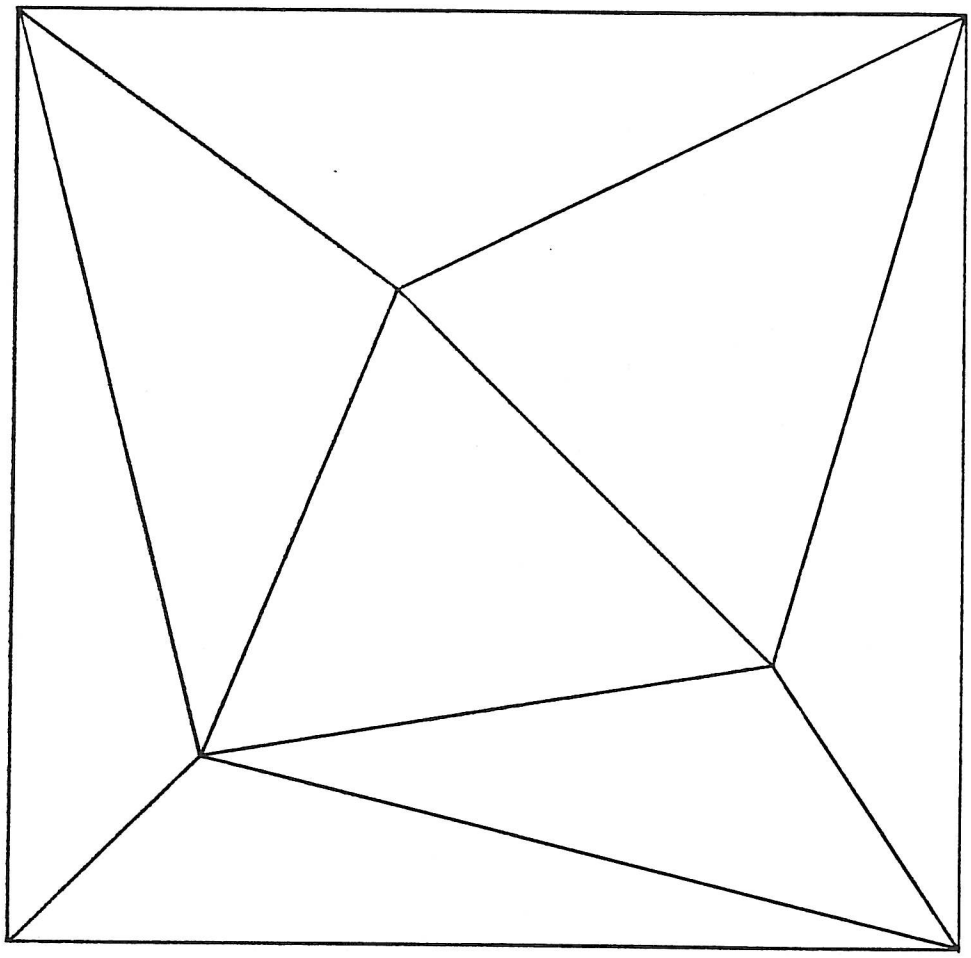

Fig. 5.1 Patch test mesh

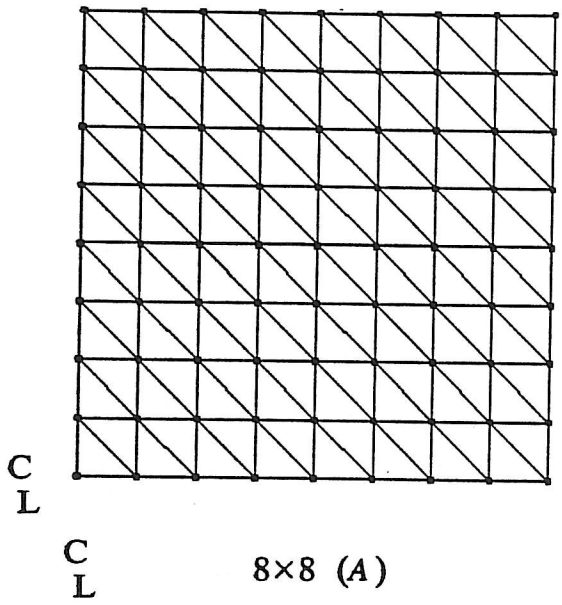

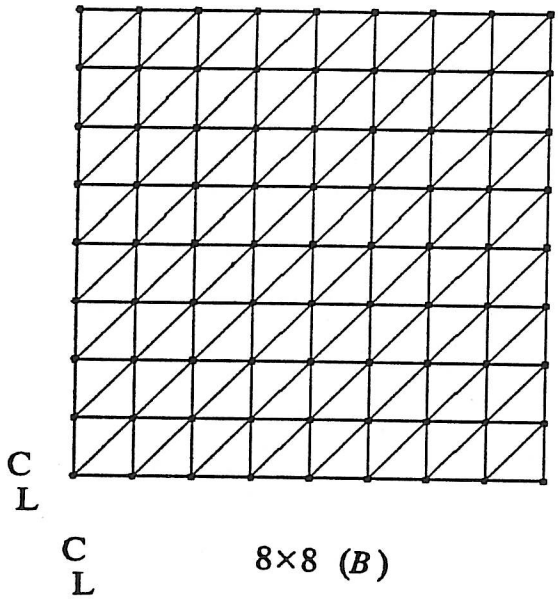

Fig. 5.1.1 Square plate meshes

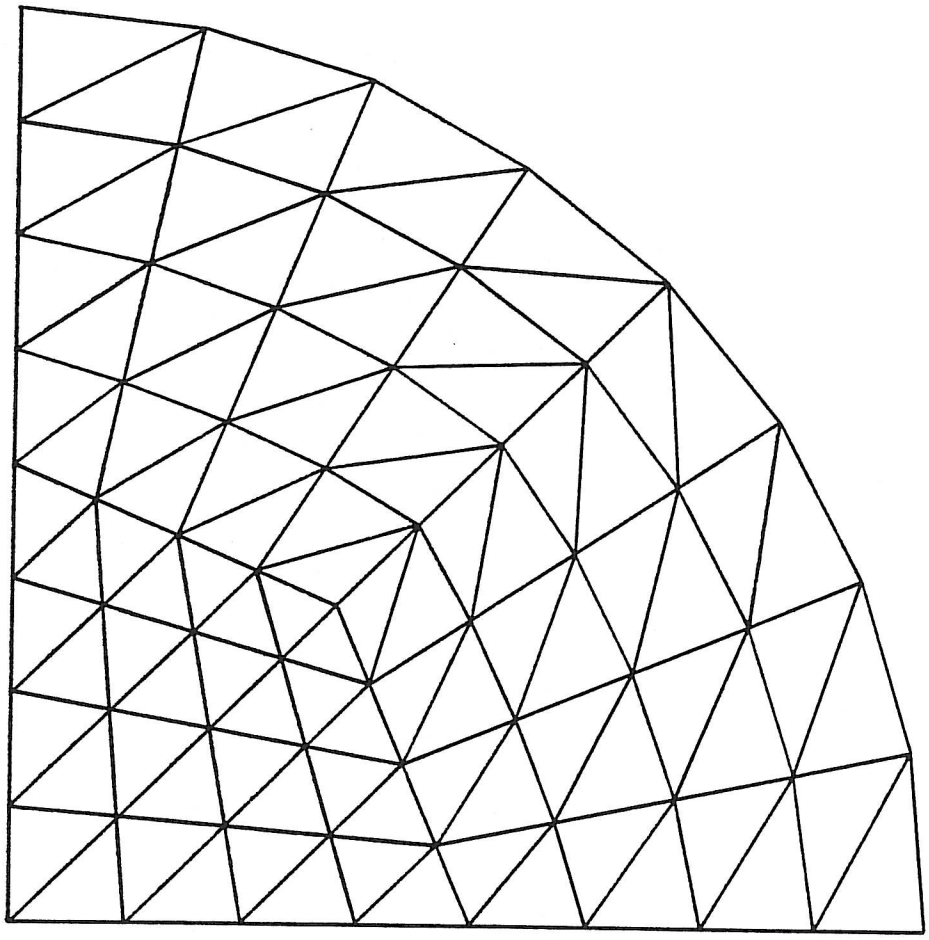

96 elements

Fig. 5.2.1 Typical circular plate mesh

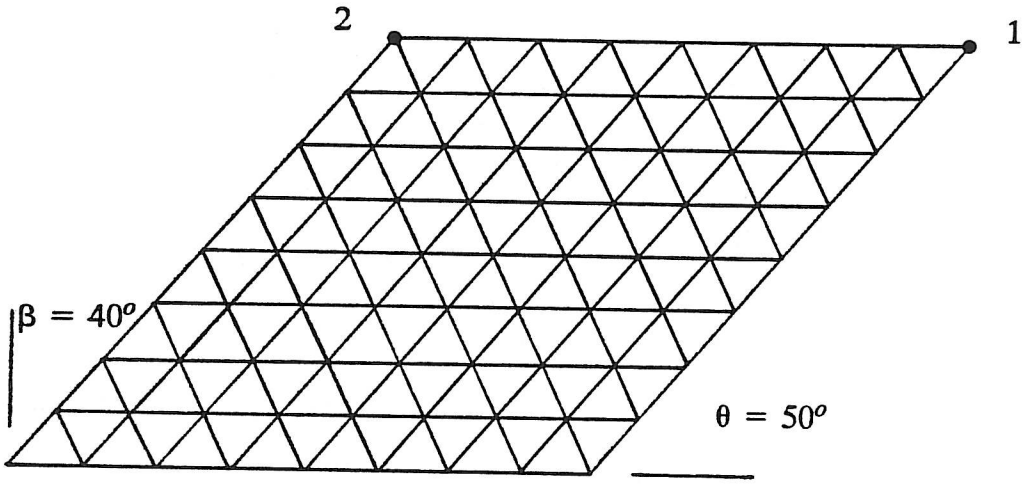

8×8 (A)

Fig. 5.3.1 Typical cantilever skew plate mesh

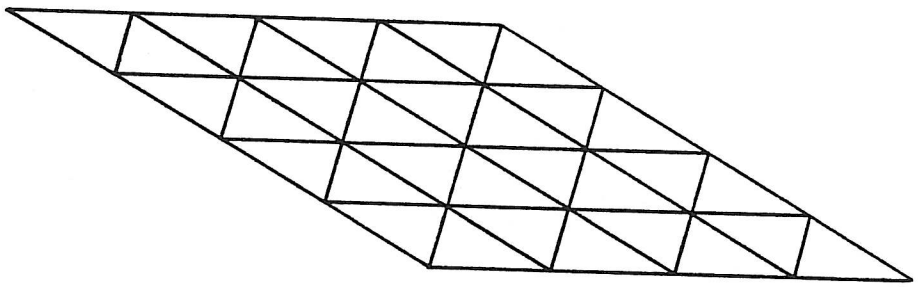

4×4

Fig. 5.4.1 Simply supported skew plate mesh

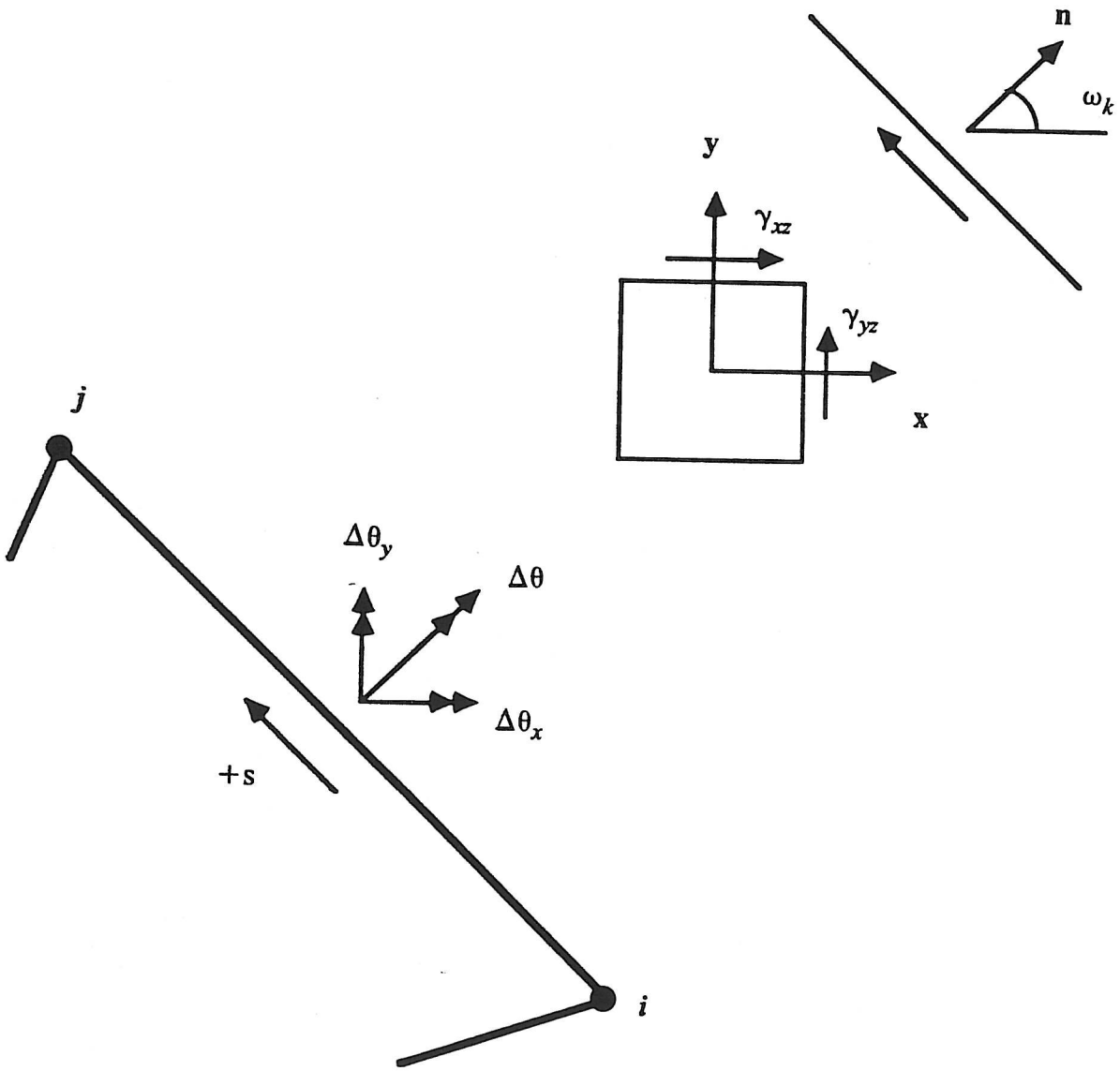

Fig. A.1 Evaluation of the tangential shear along an edge